galaxies

MDPI

Conference Report

On the Spectrum and Polarization of Magnetar Flare Emission

Roberto Taverna [1,2,*] and Roberto Turolla [1,3]

1 Department of Physics and Astronomy, University of Padova, via Marzolo 8, I-35131 Padova, Italy
2 Department of Mathematics and Physics, University of Roma 3, via della Vasca Navale 84, I-00146 Roma, Italy
3 Mullard Space Science Laboratory, University College London, Holmbury St. Mary, Surrey RH5 6NT, UK; turolla@pd.infn.it
* Correspondence: taverna@pd.infn.it

Received: 31 January 2018; Accepted: 28 February 2018; Published: 12 March 2018

Abstract: Bursts and flares are among the distinctive observational manifestations of magnetars, isolated neutron stars endowed with an ultra-strong magnetic field ($B \approx 10^{14}$–10^{15} G). It is believed that these events arise in a hot electron-positron plasma, injected in the magnetosphere, due to a magnetic field instability, which remains trapped within the closed magnetic field lines (the "trapped-fireball" model). We have developed a simple radiative transfer model to simulate magnetar flare emission in the case of a steady trapped fireball. After dividing the fireball surface in a number of plane-parallel slabs, the local spectral and polarization properties are obtained integrating the radiative transfer equations for the two normal modes. We assume that magnetic Thomson scattering is the dominant source of opacity, and neglect contributions from second-order radiative processes, although the presence of double-Compton scattering is accounted for in establishing local thermal equilibrium in the fireball atmospheric layers. The spectra we obtained in the 1–100 keV energy range are in broad agreement with those of available observations. The large degree of polarization ($\gtrsim$80%) predicted by our model should be easily detectable by new-generation X-ray polarimeters, like *IXPE*, *XIPE* and *eXTP*, allowing one to confirm the model predictions.

Keywords: polarization; radiative transfer; scattering; techniques: polarimetric; stars: magnetars; X-rays: bursts

1. Introduction

Magnetars are a particular kind of isolated neutron stars (NSs), observationally identified with Soft Gamma Repeaters (SGRs) and Anomalous X-ray pulsars (AXPs). One of the most distinctive properties of these sources is the emission of short ($\approx 10^{-2}$–1 s) energetic ($\approx 10^{36}$–10^{41} erg) X-ray bursts and longer ($\approx$1–50 s), even more energetic ($\approx 10^{41}$–10^{43} erg) intermediate flares; three SGRs have been observed to also emit giant flares, the most powerful events ever observed from compact objects (10^{44}–10^{47} erg, see [1,2] for reviews), composed by a short ($\approx$1 s) initial spike followed by a long ($\approx$1000 s) pulsating tail, modulated at the spin frequency of the star. According to the magnetar model, first developed by [3], the huge internal magnetic field of magnetars is believed to develop a large toroidal component, which exerts a strong magnetic stress on the conductive star crust. In contrast to what happens in 'normal' NSs, where this force can be balanced by the rigidity of the crust, in magnetars the internal stresses are strong enough to displace single surface elements. As a result, the external magnetic field acquires in turn a non-zero toroidal component, becoming twisted, and this makes possible for charged particles to fill the magnetosphere, streaming along the closed field lines [4,5]. Although the mechanisms that trigger magnetar bursting activity are still not completely clear, Thompson and Duncan [6,7] suggested a model according to which magnetar flares originate in

the sudden re-arrangements of the external field lines that follow the crustal displacements triggered by the strong internal field. This injects in the magnetosphere an Alfvén pulse that dissipates into an electron-positron pair plasma, which remains magnetically confined within the closed field lines (the "trapped fireball").

In this work we study the spectral and polarization properties of the radiation emitted from a steady trapped fireball, providing simulations directly comparable with observations (see [8]). Although our model relies on a series of simplifying assumptions, the simulated spectra we obtained in the 1–100 keV energy range, that can be suitably described in terms of the superposition of two blackbodies, turn out to be in broad agreement with the observations available so far [9–11]. The large degree of polarization expected for magnetar burst radiation can be easily measured by new-generation X-ray polarimeters, such as *IXPE*, *XIPE* and *eXTP*, that will allow to confirm the model predictions. We discuss the details of our model in Section 2; the radiative processes which take place in the fireball medium are described in Section 2.1, while in Sections 2.2 and 2.3 we deal with the problem of radiative transfer and describe the structure of our numerical codes. The results of our simulations are presented in Section 3, while discussion and conclusions are reported in Section 4.

2. The Model

2.1. Radiative Processes in Strong Magnetic Fields

We assume magnetic scattering as the main source of opacity in the fireball medium. For the sake of simplicity, we consider scattering in the Thomson limit; the full case of Compton scattering will be addressed in a sequel work (exact expressions for Compton scattering cross-sections have been derived in [12–14]). Strong magnetic fields of magnetars are expected to linearly polarize the photons emitted from the surface in two normal modes, the ordinary (O) and the extraordinary (X), with the polarization vector oscillating either parallel or perpendicular to the $(\boldsymbol{k}, \boldsymbol{B})$ plane, being $\boldsymbol{k}$ the photon propagation direction and $\boldsymbol{B}$ the star magnetic field [15–17]. In the hypothesis (well verified for magnetar bursts) that the photon energy ε is much smaller than the electron cyclotron energy $\varepsilon_\mathrm{B} = m_\mathrm{e}c^2 B/B_\mathrm{Q}$, with m_e the electron mass, scattering of photons onto electrons/positrons is non-resonant. In the electron rest frame, and neglecting the electron recoil, the scattering cross-sections depend on the polarization state of both the ingoing and the outgoing photons [18–20]:

$$\left[\frac{\mathrm{d}^2\sigma}{\mathrm{d}\varepsilon'\mathrm{d}\Omega'}\right]_{\mathrm{OO}} = \frac{3}{8\pi}\sigma_\mathrm{T}\left(1-\mu_\mathrm{Bk}^2\right)\left(1-\mu_\mathrm{Bk}'^2\right)\delta\,, \qquad \left[\frac{\mathrm{d}^2\sigma}{\mathrm{d}\varepsilon'\mathrm{d}\Omega'}\right]_{\mathrm{OX}} = \frac{3}{8\pi}\sigma_\mathrm{T}\left(\frac{\varepsilon}{\varepsilon_\mathrm{B}}\right)^2\mu_\mathrm{Bk}^2\nu_\mathrm{Bk}^2\delta\,,$$

$$\left[\frac{\mathrm{d}^2\sigma}{\mathrm{d}\varepsilon'\mathrm{d}\Omega'}\right]_{\mathrm{XO}} = \frac{3}{8\pi}\sigma_\mathrm{T}\left(\frac{\varepsilon}{\varepsilon_\mathrm{B}}\right)^2\mu_\mathrm{Bk}'^2\nu_\mathrm{Bk}^2\delta\,, \qquad \left[\frac{\mathrm{d}^2\sigma}{\mathrm{d}\varepsilon'\mathrm{d}\Omega'}\right]_{\mathrm{XX}} = \frac{3}{8\pi}\sigma_\mathrm{T}\left(\frac{\varepsilon}{\varepsilon_\mathrm{B}}\right)^2(1-\nu_\mathrm{Bk}^2)\delta\,, \tag{1}$$

where a prime labels the quantities after scattering, σ_T is the Thomson cross section, μ_Bk is the cosine of the angle θ_Bk between the photon direction and the local magnetic field, ν_Bk is the cosine of the associated azimuth ϕ_Bk and $\delta = \delta(\varepsilon - \varepsilon')$ is the Dirac δ-function. The previous expressions hold as far as the vacuum contributions in the dielectric tensor dominate over the plasma ones [21]. As it is evident from Equation (1), all the cross-sections involving X-mode photons are suppressed by a factor of $(\varepsilon/\varepsilon_\mathrm{B})^2 \propto (\varepsilon B_\mathrm{Q}/B)^2$ with respect to the O–O cross-section, which is essentially of the order of σ_T. This implies that the medium becomes optically thin for extraordinary photons at much larger Thomson depths with respect to the ordinary ones.

Among the additional second-order processes that can take place in magnetized plasma there are thermal bremsstrahlung, photon splitting and double-Compton scattering. The bremsstrahlung between particles with the same charge becomes important only for high particle energies (above 300 keV, see [22], outside the range we considered in our work), so that only the electron-positron bremsstrahlung, slightly enhanced with respect to the electron-ion one [23,24], turns out to be relevant

under our assumptions. Also in this case, however, the amplitude of the process is negligible for magnetar burst radiation, allowing to neglect the contributions of thermal bremsstrahlung in our work. Moreover, although photon splitting can be important in a wider range of photon energies [25,26], the cross section of the process turns out to be much smaller than $\sigma_{\rm T}$ in the weak-field limit (and for photon energies $\lesssim$100 keV), while one should consider an additional suppression factor in the strong-field limit [27,28]. For these reasons we have safely neglected also photon splitting effects in the model.

In the light of this, double-Compton scattering is the unique process responsible for photon production in the fireball in our model. According to [29], for large scattering depths photons follow a Planck distribution at energies low enough to make double-Compton scattering dominant, while at higher energies scattering tends to establish a Bose-Einstein distribution. However, as shown by [30], the photon chemical potential remains rather small, allowing to solve the photon transport assuming local thermal equilibrium (LTE) at large depth for both O- and X-mode photons [8].

2.2. Radiative Transfer in the Fireball Atmosphere

We solved the radiative transfer equations for both the ordinary and the extraordinary photons in the geometrically thin surface layers of the fireball, which we term the atmosphere. The latter is divided into a number of patches, each labelled by the intensity of the magnetic field at the patch centre and by the angle $\theta_{\rm B}$ between $\boldsymbol{B}$ and the local normal $\boldsymbol{z}$. Once the viewing geometry is set, i.e., the angles χ and ξ that the star rotation axis Ω makes with the observer line-of-sight (LOS) and the star magnetic axis, respectively, the contributions of all the patches in view are summed together to derive the spectral and polarization properties of the emitted radiation. We also assume that the patch dimensions are small enough with respect to the radial scale to neglect the curvature of the closed field lines that contain the fireball, so that we can treat the atmosphere in the plane-parallel approximation. Under these assumptions the radiative transfer equations assume a relatively simple form,

$$\mu_z \frac{{\rm d}n_i}{{\rm d}\tau} = C_i n_i - S_i \,, \tag{2}$$

where n_i are the photon number intensities ($i = {\rm O, X}$), ${\rm d}\tau$ is the infinitesimal Thomson depth, μ_z is the cosine of the angle between the photon direction and the local normal, C_i are terms that do not depend on τ and S_i represents the source terms. Due to the suppression factor B^{-2} that affects the X-mode cross sections (see Equation (1)), integrating the equations for the Thomson depth could require long computational times. In particular, the X-mode photosphere will lie at different heights in the fireball atmosphere for different photon energies, while at the same time the medium remains optically thick for ordinary photons at all the photon energies. For these reasons, we adopted the approach used by [30], solving the radiative transfer equations in terms of the Rosseland mean optical depth $\tau_{\rm R}$, which is related to the Rosseland mean cross section $\sigma_{\rm X} = \sigma_{\rm XX} + \sigma_{\rm XO}$ of the X-mode photons.

2.3. Numerical Implementation

We developed a specific FORTRAN code to solve the radiative transfer in the fireball atmosphere. We assumed a maximum optical depth $\tau_{\rm R}^{\rm max} = 1000$ at the base of the atmosphere, since this guarantees that the medium is optically thick for X-mode photons over the entire energy range 1–100 keV, up to $\tau_{\rm R}^{\rm min} = 0$ at the top. Under these conditions, the typical number density at the base of the fireball is $\sim 10^{26}$ cm^{-3} (see also [31]). A good approximation for the temperature distribution in a scattering-dominated medium in the diffusion regime turns out to be $T = T_{\rm b}(1 + 0.75\tau_{\rm R})^{1/2}$ [30], where $T_{\rm b}$ is the bolometric temperature (we assumed $T_{\rm b} = 10$ keV, so that the temperature ranges from $\sim$280 keV at the base of the fireball and 10 keV on the top). We checked a posteriori that this provides a good approximation to the numerical solution one obtains solving the energy balance in the fireball also at small optical depths. Deviations turn out to be less than 15 per cent, in agreement with what found also by [30]. Using this temperature distribution, one can simply relate the Thomson

scattering depths τ_O and τ_X for O- and X-mode photons, respectively, to the Rosseland mean optical depth. At the base of the fireball the large optical depth ensures that both ordinary and extraordinary photon distributions are isotropic blackbodies. In order to avoid too long runs, we decide to integrate the two radiative transfer equations for $\tau_{O,X} \leq 10$ only, taking $n_{O,X}$ as Planck distributions at the local temperature T otherwise. Since, for the chosen values of the parameters, the X-mode photosphere lies always at larger τ_R with respect to the O-mode one, we solve the transfer equation for only n_X in the case of $\tau_X \leq 10$ and $\tau_O > 10$, taking n_O as Planckian [8,30]. For the sake of simplicity, we assume the external magnetic field as dipolar, with polar intensity $B_p = 10^{14}$ G; the fireball is then limited by the close field lines that reach a maximum distance R_{max} from the star, taken as twice the stellar radius $R_{NS} = 10$ km. For this reason, all the patches in which the fireball atmosphere is divided are characterized by an angle $\theta_B = 90°$.

In order to sum together the contributions coming from all the patches in view, we used an IDL ray-tracing code [8,32,33]. Once the viewing angles χ and ξ have been chosen, the code solves the terminator condition $\boldsymbol{z} \cdot \boldsymbol{\ell} = 0$, where $\boldsymbol{z}$ is the fireball surface normal and $\boldsymbol{\ell}$ is the unit vector of the observer LOS, to determine the points of the fireball surface which enter into view at different rotational phases. Since in general the fireball terminator shape turns out to be quite complicate, we decide to neglect the general relativistic corrections in our code. Nevertheless, as we checked in previous works (see [32]), general relativity marginally influences the behavior of the polarization observables at infinity, and the qualitative conclusions we discuss in the following hold in general. Finally, we considered two different emission geometries, the model a, in which photons come from the entire torus limited by the field lines that enclose the fireball, and the model b, in which the emitting region is only a portion of this torus. In this latter case, radiation emitted from the planar slices that limit the emitting part of the torus is also considered (see Figure 1). QED effects on the polarization modes are treated as discussed in [32,34]; in particular, since we assumed the vacuum contributions to the dielectric tensor as dominant with respect to the plasma ones, vacuum resonance effects turn out to be negligible in our model for photon energies above 1–2 keV.

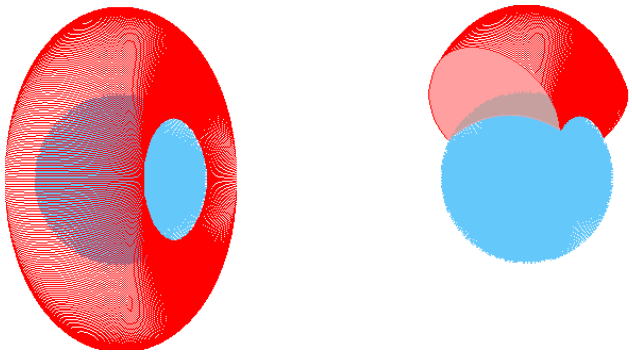

Figure 1. Limiting field lines (red solid lines) of a torus-shaped fireball in the case of model a (**left-hand side**) and model b (with angular opening $\Delta\phi = 90°$, **right-hand side**). In the latter case, one of the two planar slices that limit the emitting part of the torus is also shown (faded-red region).

3. Results

The intensities calculated in the radiative transfer code and processed in the ray-tracer are then used to obtain the simulated spectra and the polarization observables (both phase-resolved and phase-averaged) as observed at infinity. Since observations of the 'burst forest' emitted by SGR 1900+14 in 2006 [9] suggest that the spectrum of the intermediate flares (and of normal bursts too) is thermal and well reproduced by the superposition of two blackbodies, we attempted to fit the phase-averaged spectra with two Planckian distributions (with temperatures T_1 and T_2 and normalizations A_1 and A_2), although comparing results from our simplified model with real observations could be premature. Figure 2 shows the phase-averaged total spectrum of the radiation emitted from the fireball in the

case of a limited emitting region (model b) with angular opening $\Delta\phi = 90°$, for $\chi = 60°$ and $\xi = 30°$, together with the best fit and the single blackbody components (see [8] for further details). Under our assumptions, the values of T_1 and T_2 as well as of the ratio A_2/A_1 turn out to be in broad agreement with observations, though the temperature of the softer component (∼2 keV) turns out to be somehow lower than the observed one (∼5 keV). No significant difference is expected switching from model a to model b or changing the viewing geometry. Moreover, we found that our model is able to reproduce the typical pulsating profile of the observed magnetar flare decay tails, even if in the case of model a this is possible whenever the fireball is seen under a favorable viewing geometry (see, e.g., Figure 3).

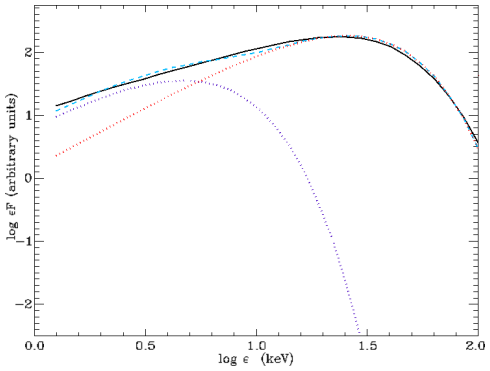

Figure 2. Phase-averaged photon spectrum (black solid line) of the radiation emitted in the case of model b (with $\Delta\phi = 90°$), fitted by the superposition of two blackbody components for $\chi = 60°$ and $\xi = 30°$. The best fit is marked by the light-blue dashed line, and the single blackbody components at themperatures T_1 (blue dotted line) and T_2 (red dotted line) are also shown.

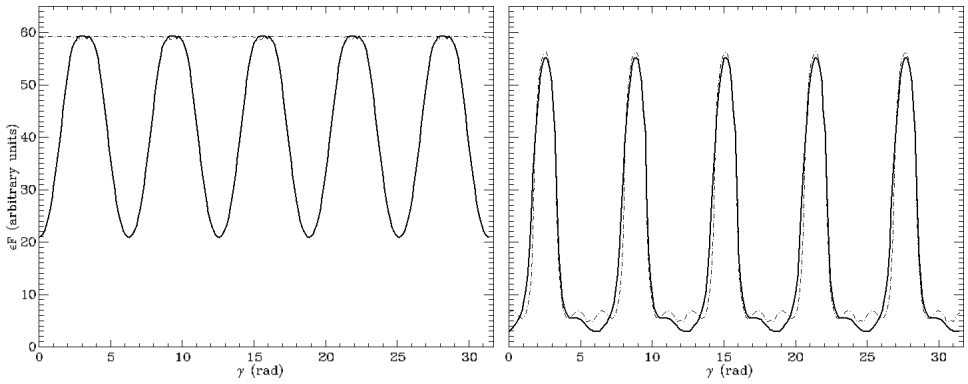

Figure 3. Pulse profile of the radiation emitted from the fireball in the case of model a (**left-hand panel**) and model b (with $\Delta\phi = 90°$, **right-hand panel**), calculated in the 10–50 keV energy range. Here the solid lines refer to the case $\chi = 60°$, $\xi = 30°$, and the dash-dotted lines refer to the case $\chi = 90°$, $\xi = 0°$ (see [8] for further details).

The observed polarization signal, simulated taking into account both vacuum polarization and the geometrical effects due to the magnetic field topology [32], confirms that, according to our model, radiation collected from a magnetar flare is expected to be highly polarized in the extraordinary mode. In particular, the phase-resolved linear polarization fraction Π_L attains a value generally higher than 80 per cent for photon energies between 1–50 keV, while a decrease up to ∼40 per cent is expected only at higher energies (see Figure 4). This reflects the behavior of the scattering cross-sections (see Equation (1)), according to which X-mode photons dominate the spectrum at almost all the photon energies, while τ_X becomes comparable with τ_O above ∼50 keV. Such a high polarization degree will be readily measurable by new-generation X-ray polarimeters like *IXPE*, *XIPE* and *eXTP*, as confimed by the simulations reported in Figure 5. Here, we refer to an event characterized by an X-ray flux

$F_X = 4.68 \times 10^{-7}$ erg cm^{-2} s^{-1} in the 1–10 keV energy range and a duration $t_{exp} = 1.737$ s, for different viewing geometries. It can be noted that both polarization fraction and angle measurements recover the values expected from the theoretical model with an acceptable degree of accuracy (within 1σ), although the errors on the polarization angle increase by decreasing the corresponding polarization degree.

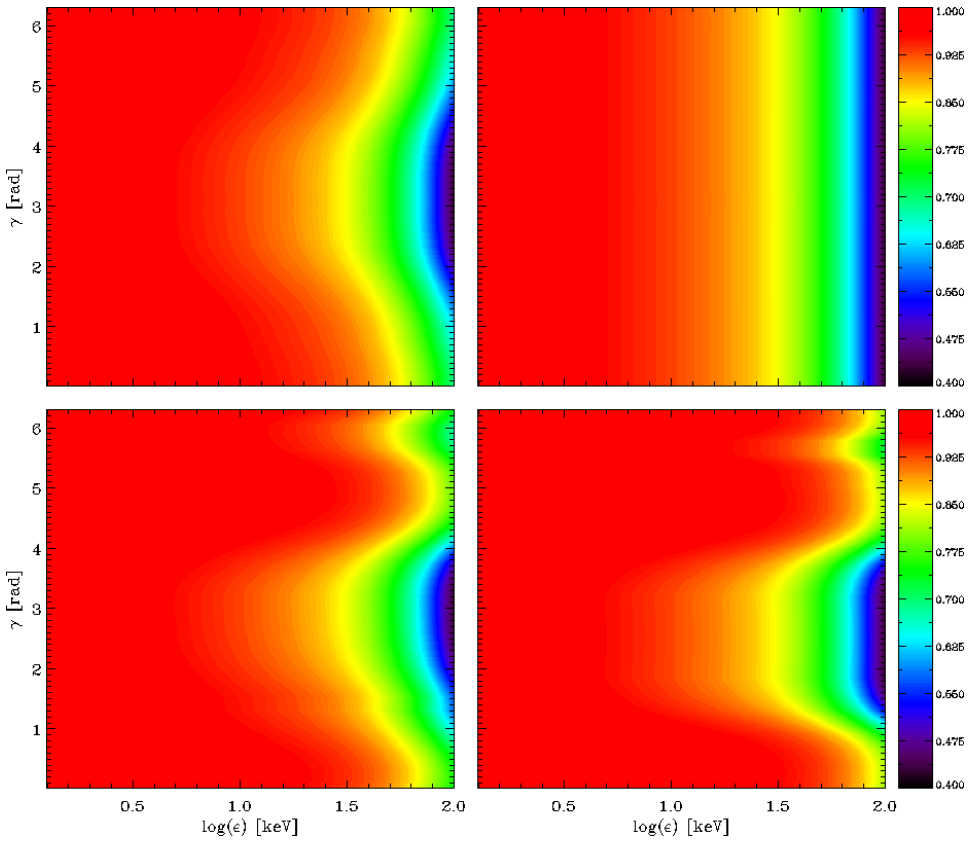

Figure 4. Contour plots of the linear polarization degree as a function of the photon energy and the rotational phase, for $\chi = 60°$, $\xi = 30°$ (**left-hand column**) and $\chi = 90°$, $\xi = 0°$ (**right-hand column**). The top row refers to model a and the bottom row refers to model b (with $\Delta\phi = 90°$, see [8] for further details).

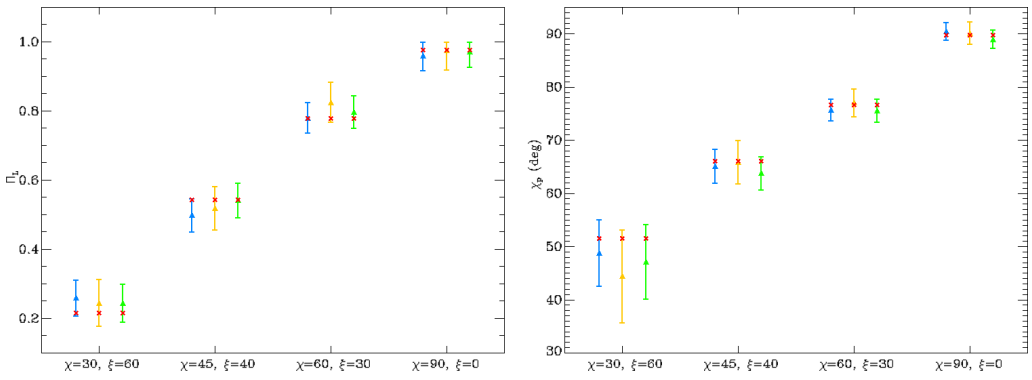

Figure 5. Simulation (triangles with error bars) of the phase-averaged linear polarization fraction (**left-hand panel**) and polarization angle (**right-hand panel**) of the *XIPE* (blue), *IXPE* (orange) and *eXTP* (green) polarimeters to the signal predicted by our theoretical model (in the case of model b) for a duration $t_{exp} = 1.737$ s, X-ray flux $F_X = 4.68 \times 10^{-7}$ erg cm^{-2} s^{-1} in the 1–10 keV energy range and different viewing geometries (red crosses).

4. Conclusions

We have revisited the problem of modelling the spectral and polarization properties of the radiation emitted during magnetar flares in the context of the trapped-fireball model [6,7]. Our code integrates the radiative transfer equations for both ordinary and extraordinary photons in the fireball atmospheric layer, divided into a number of different patches. This model generalizes the approach presented in [30], where only the case of $\boldsymbol{B}$ parallel to the patch normal was treated. The outputs of the FORTRAN radiative transfer code have been reprocessed through an IDL ray-tracing code, in order to obtain the spectra and the polarization observable distributions as measured by a distant observer. The results we obtained from the spectral analysis are compatible with observations, also in reproducing the typical pulse profile of magnetar flare decay tails. We point out that including general relativistic effects would modify the shape of the lightcurves shown in Figure 3, also lowering the pulsed fraction. Our goal here was just to show that pulsations can be produced in our model, with a pulsed fraction that depends on both the observer inclination and the emission geometry. We also note that the effects of non-conservative scattering would modify the high-energy part of the spectrum, likely producing a comptonization tail. Finally, the model predicts a high degree of polarization, that promises to be readily detected through phase-resolved measurements with the polarimetric missions under development, allowing to verify the predictions of our theoretical model.

Author Contributions: The authors contributed equally to this work.

Conflicts of Interest: The authors declare no conflict of interest.

Abbreviations

The following abbreviations are used in this manuscript:

IXPE	Imaging X-ray Polarimetry Explorer
XIPE	X-ray Imaging Polarimetry Explorer
eXTP	Enhanced X-ray Timing and Polarimetry mission
NS	Neutron Star
SGR	Soft Gamma Repeater
AXP	Anomalous X-ray Pulsar
O-mode	Ordinary mode
X-mode	Extraordinary mode
LTE	Local Thermal Equilibrium
LOS	Line-Of-Sight

References

1. Mereghetti, S. The strongest cosmic magnets: Soft gamma-ray repeaters and anomalous X-ray pulsars. *Astron. Astrophys. Rev.* **2008**, *15*, 225–287.
2. Turolla, R.; Zane, S.; Watts, A.L. Magnetars: The physics behind observations. A review. *Rep. Prog. Phys.* **2015**, *78*, 116901.
3. Duncan, R.C.; Thompson, C. Formation of very strongly magnetized neutron stars-Implications for gamma-ray bursts. *Astrophys. J.* **1992**, *392*, L9–L13.
4. Thompson, C.; Lyutikov, M.; Kulkarni, S.R. Electrodynamics of magnetars: Implications for the persistent X-ray emission and spin-down of the soft gamma repeaters and anomalous X-ray pulsars. *Astrophys. J.* **2002**, *574*, 332.
5. Nobili, L.; Turolla, R.; Zane, S. X-ray spectra from magnetar candidates—I. Monte Carlo simulations in the non-relativistic regime. *Mon. Not. R. Astron. Soc.* **2008**, *386*, 1527–1542.
6. Thompson, C.; Duncan, R.C. Radiative mechanism for outbursts. *Mon. Not. R. Astron. Soc.* **1995**, *275*, 255–300.
7. Thompson, C.; Duncan, R.C. The giant flare of 1998 August 27 from SGR 1900+14. II. Radiative mechanism and physical constraints on the source. *Astrophys. J.* **2001**, *561*, 980.

8. Taverna, R.; Turolla, R. On the spectrum and polarization of magnetar flare emission. *Mon. Not. R. Astron. Soc.* **2017**, *469*, 3610–3628.
9. Israel, G.L.; Romano, P.; Mangano, V.; Dall'Osso, S.; Chincarini, G.; Stella, L.; Campana, S.; Belloni, T.; Tagliaferri, G.; Blustin, A.J.; et al. A swift gaze into the 2006 March 29 burst forest of SGR 1900+14. *Astrophys. J.* **2008**, *685*, 1114.
10. Olive, J.-F.; Hurley, K.; Sakamoto, T.; Atteia, J.L.; Crew, G.; Ricker, G.; Pizzichini, G.; Barraud, C.; Kawai, N. Time-resolved X-ray spectral modeling of an intermediate burst from SGR 1900+14 observed by HETE-2 FREGATE and WXM. *Astrophys. J.* **2004**, *616*, 1148.
11. Feroci, M.; Caliandro, G.A.; Massaro, E.; Mereghetti, S.; Woods, P.M. Broadband X-ray spectra of short bursts from SGR 1900+ 14. *Astrophys. J.* **2004**, *612*, 408.
12. Daugherty, J.K.; Harding, A.K. Compton scattering in strong magnetic fields. *Astrophys. J.* **1986**, *309*, 362–371.
13. Gonthier, P.L.; Harding, A.K.; Baring, M.G.; Costello, R.M.; Mercer, C.L. Compton scattering in ultrastrong magnetic fields: Numerical and analytical behavior in the relativistic regime. *Astrophys. J.* **2000**, *540*, 907.
14. Mushtukov, A.A.; Nagirner, D.I.; Poutanen, J. Compton scattering S matrix and cross section in strong magnetic field. *Phys. Rev. D* **2016**, *612*, 93–119.
15. Gnedin, Y.N.; Pavlov, G.G. The transfer equations for normal waves and radiation polarization in an anisotropic medium. *J. Exp. Theor. Phys.* **1974**, *38*, 903–908.
16. Ho, W.C.G.; Lai, D. Atmospheres and spectra of strongly magnetized neutron stars—II. The effect of vacuum polarization. *Mon. Not. R. Astron. Soc.* **2003**, *338*, 233–252.
17. Lai, D.; Ho, W.C.G.; van Adelsberg, M.; Wang, C.; Heyl, J.S. *X-ray Polarimetry: A New Window in Astrophysics*; Cambridge University Press: Cambridge, UK, 2010.
18. Herold, H. Compton and Thomson scattering in strong magnetic fields. *Phys. Rev. D* **1979**, *19*, 2868.
19. Ventura, J. Scattering of light in a strongly magnetized plasma. *Phys. Rev. D.* **1979**, *19*, 1684.
20. Mészáros, P. *High-Energy Radiation from Magnetized Neutron Stars*; University Chicago Press: Chicago, IL, USA, 1992.
21. Harding, A.K.; Lai, D. Physics of strongly magnetized neutron stars. *Rep. Prog. Phys.* **2006**, *69*, 2631.
22. Haug, E. Bremsstrahlung and pair production in the field of free electrons. *Z. Naturforsch. A* **1975**, *30*, 1099–1133.
23. Svensson, R. Electron-positron pair equilibria in relativistic plasmas. *Astrophys. J.* **1982**, *258*, 335.
24. Haug, E. Electron-positron bremsstrahlung in mildly relativistic thermal plasmas. *Astron. Astrophys.* **1985**, *148*, 386–390.
25. Adler, S.L.; Bahcall, J.N.; Callan, C.G.; Rosenbluth, M.N. Photon splitting in a strong magnetic field. *Phys. Rev. Lett.* **1970**, *25*, 1061.
26. Adler, S.L. Photon splitting and photon dispersion in a strong magnetic field. *Ann. Phys. N. Y.* **1971**, *67*, 599–647.
27. Stoneham, R.J. Phonon splitting in the magnetised vacuum. *J. Phys. A* **1979**, *12*, 2187.
28. Bulik, T. Photon splitting in strongly magnetized plasma. *Acta Astron.* **1998**, *48*, 695.
29. Lightman, A. Double Compton emission in radiation dominated thermal plasmas. *Astrophys. J.* **1981**, *244*, 392–405.
30. Lyubarsky, Y.E. On the X-ray spectra of soft gamma repeaters. *Mon. Not. R. Astron. Soc.* **2002**, *332*, 199–204.
31. Yang, Y.-P.; Zhang, B. On the polarization properties of magnetar giant flare pulsating tails. *Astrophys. J.* **2015**, *815*, 45.
32. Taverna, R.; Turolla, R.; González Caniulef, D.; Zane, S.; Muleri, F.; Soffitta, P. Polarization of neutron star surface emission: A systematic analysis. *Mon. Not. R. Astron. Soc.* **2015**, *454*, 3254–3266.
33. Zane, S.; Turolla, R. Unveiling the thermal and magnetic map of neutron star surfaces though their X-ray emission: Method and light-curve analysis. *Mon. Not. R. Astron. Soc.* **2006**, *366*, 727–738.
34. Taverna, R.; Muleri, F.; Turolla, R.; Soffitta, P.; Fabiani, S.; Nobili, L. Probing magnetar magnetosphere through X-ray polarization measurements. *Mon. Not. R. Astron. Soc.* **2014**, *438*, 1686–1697.